Electronic structure of Thiolate Self-Assembled Monolayers on Cu(111) and Au(111) substrates.

Vasili Perebeinos[1] and Marshall Newton[2]

[1]*Department of Physics,*

[2]*Department of Chemistry,*

Brookhaven National Laboratory,

Upton, New York 1973-5000

(Dated: June 25, 2003)

Abstract

Recently there has been increased interest in the possibility of using organic molecules as possible electronic components in nanoscale devices. One of the most important issues to be addressed is the role of molecule-surface interactions. We use first principles density functional theory to calculate electronic structure of the thiophenolate (SC_6H_5) Self-Assembled monolayer (SAM) on Cu(111) and Au(111) substrates. We find lateral dispersion of the molecular states comparable to the charge injection energy at Γ point, which suggests that the conductance of the SAM is significantly different from that of the single molecule. We calculate the two photon photoemission spectra (2PPE) and comparer with the available experimental data. Our results allows reinterpretation of the available data and contains prediction for new electronic states due to the monolayer not yet accessed experimentally.

PACS numbers:

I. INTRODUCTION

The purpose of this paper is to elucidate the electronic structure of molecular electronic states attached at the noble metal substrate. At the molecule-metal interface the charge redistribution equilibrates the chemical potentials in two systems. The key quantity which controls the conductance properties of the interface is the relative position of the Fermi level on a metal and the molecular states available for the transport. In the case of the single molecule attached to the metal substrate the molecular state has an well define energy and the life time broadening due to the finite lifetime, which is controlled by the coupling to the substrate. In the case of the monolayer the molecular orbitals form a two dimensional band structure due to the finite overlap between the orbitals on different orbitals. When the spacing between the molecules is large the band width gets small and negligible at the infinite separation between the molecules. Additional source of the lateral dispersion is the substrate mediated superexchange type interaction. The latter has a weaker distance dependence than the direct overlap which decays exponentially with a separation. In these studies we calculate lateral dispersion of the thiophenolate attached to the Cu(111) and Au(111). We aim to answer three essential questions: (1) to what molecular state the charge injection energy is minimal and therefore the most significant for the conduction properties through the monolayer; (2) how large is the lateral dispersion compared to the charge injection energy at Γ point which corresponds to a single molecule attachment; (3) what the relative contribution of the direct overlap and substrate mediated interaction to the dispersion. From the experimental end the thiolate on Cu(111) system has been studied using two photon photoemsition (2PPE) techniques [1]. The Zhu's group reports a work function shift from 4.9 eV for the clean Cu surface to 3.7 eV with the adsorbed SAM. Additionally, two states were resolved, one at 3.3 eV and the other at 6.4 eV relative to the Fermi level.

II. METHOD OF CALCULATION

We use the general potential linearized augmented plane wave (FP-LAPW) method [2] with local orbital extensions [3] in the WIEN2k implementation [4]. The LDA Perdew Wang [5] exchange-correlation potential was used. Well converged basis sets were employed with

a 4.7 Ry plane wave cut off. Five special k-points were used to sample two dimensional Brillouin zone. The thiophenolate self assemble on Au(111) substrate in a so called $\sqrt{3} \times \sqrt{3}R30^0$ two dimensional structure [6]. The lattice constant of the underlying substrate controls the area per molecule which is 21.6 Å^2 for Au and 16.9 Å^2 for Cu. The free standing array of thiophenolate prefers area of 21.1 Å^2 [6]. We used slab calculations with a super cell with three atomic layers covered by a thiophenolate SC_6H_5 monolayer for electronic structure calculations and six atomic layers with two sides covered for the work function calculations. The geometry of the molecular array has been fully relaxed on an unrelaxed substrate with metal atoms in ideal crystal positions. The monolayer on Au substrate was found tilted by 18^0 in agreement with experiment [7]. The energy versus tilt angle is shown on Fig. 1. The energy difference between the global minimum and a local minimum with a monolayer vertical to the surface is comparable to the room temperature, such that large fluctuations in the value of the angle are expected at room temperature. The bridge binding site for sulfur was found in agreement with results obtained by Selloni group [8] for the alkanethiols. In the case of Cu substrate we find zero tilt angle for the monolayer due to the close spacing controlled by the lattice constant of the substrate. In addition we find an absolute minimum when the sulfur binds to the holo-1 site (where sulfur has four first neighbor Cu atoms). Binding energy for the holo-2 site (where S has three first neighbor Cu atoms) is only 10 meV higher in energy, whereas bridge site is higher in energy by 170 meV.

III. BAND STRUCTURE RESULTS

When a monolayer of thiolate self assembles on noble metal substrate the molecular levels acquire lateral dispersion due to the direct overlap between the molecules and the substrate mediated interaction. The direct overlap falls off faster with distance between the neighboring molecules than the substrate mediated interactions. In this work we use DFT to study the relative importance of the two sources and the overall magnitude of the molecular level bandwidths. The electronic structure along the high symmetry direction of the 2-D Brillouin zone is shown on Fig. (2) for the thiophenolate SAM on Cu(111). In order to distinguish which bands are originated due to the SAM and which are due to the metallic substrate we calculate projected density of states of each band inside the spheres around

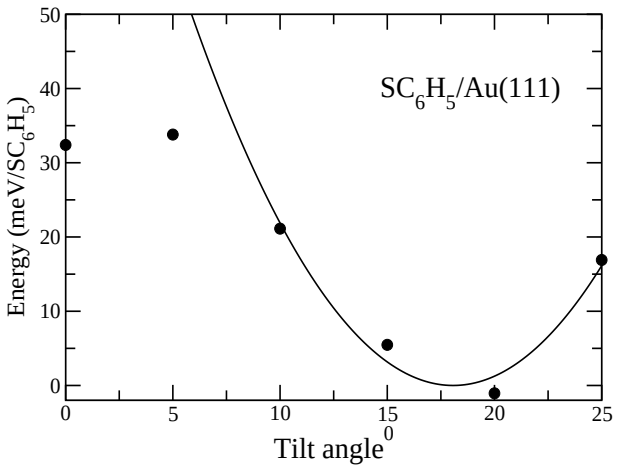

FIG. 1: Energy versus tilt angle of SC_6H_5 thiophenolate on Au substrate. The dots are the calculations and the solid line is a parabola fit with minimum angle at 18^0 and the spring constant 0.7 meV/deg^2.

each atom on a molecule. In addition the band structure of the clean Cu(111) three layer slab is shown on Fig. (2), so the new bands due to the SAM can easily be identified. Those molecular bands can be characterized by the energies at Γ-point ($k = (0, 0, 0)$), effective mass if the parabola fit in the vicinity of Γ point to the band dispersion along the Γ-M direction is possible, and the bandwidth measured as the energy difference between the M and the Γ point, and the band character. Those are given in table I. The closest to the Fermi level are the two HOMO's (H_1 and H_2) of S (3p) character. The $H_{1,2}$ bands have a very small dispersion (of about 0.2-0.3 eV) and the parabola fit results in the large effective masses of -2.0 m_e. The third occupied state (SS_{occ} at -0.9 eV) and the second unoccupied state (SS_1 at 1.7 eV) are the surface states of the covered SAM/Cu(111) . In the clean Cu(111) those states have energies 0.0 eV and -1.6 eV respectively and have similar k dispersion Fig. (1, b). Discrepancy with the experimental value of the -0.4 eV surface state energy at Γ point is due to the finite size effect of our three layer slab geometry [9]. The largest lateral dispersion is due to the bands originated from the side phenyl carbons (H_4 and L_1) separated by 2.61 Åon neighboring molecules. Other molecular bands (H_3, L_2 and L_3) are mainly due to the top and next to sulfur carbons which form triangular lattice in xy plane with side 4.42 Å. This explains why lateral dispersion of those bands is not significant compared to side carbons bands. The band between the two LUMO's L_1 and L_2 is the unoccupied surface state SS_1. Of course there are more electronic states in the band structure due to the SAM, but those are

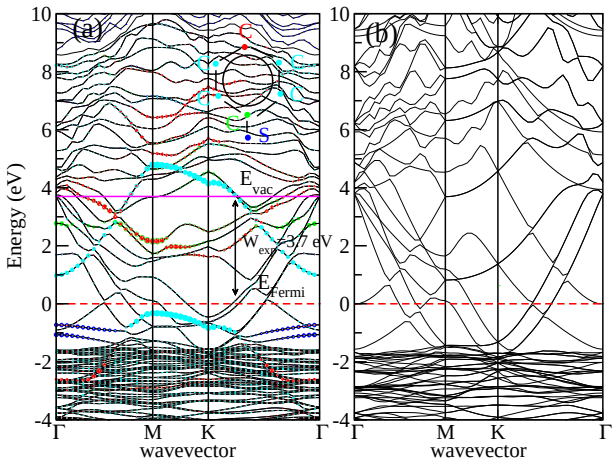

FIG. 2: (a) Band structure results for the SC_6H_5 SAM on 3 layers of Cu(111). The size of the colored circles is proportional to the projected density of states of each bend on a given atom of a molecule (sulfur S-blue, next carbon C_1-green, phenyl ring carbons $C_{2,3,5,6}$-light blue, top carbon C_6-red). (b)Band structure of the 3 layer slab of Cu(111). From comparison three HOMO bands and 3 LUMO's can be identified due to the SAM attachment.

high energy states (relative to Fermi level) and not important for the conduction properties of the monolayer. Those states are also well delocalized in space such that density of states projection inside the muffin tin spheres does not give a unique identification of the molecular bands. As it will be clear in Section IV the LUMO at 6 eV has the largest contribution to the observed two photon photoemission intensity in resonance A by Zhu's group [1].

When the thiophenolate is attached to the Au substrate the bandwidths of all molecular bands gets narrow because the next neighbor distance between molecules is larger due to the larger lattice constant of the underlying substrate. The electronic band dispersion of SAM/Au(111) and clean Au(111) surface are shown on Fig. 3. A similar band assignment can be done with the results given in table (I). As in the case of SAM on Cu the closest to the Fermi level are two nearly degenerate sulfur HOMO's ($H_{1,2}$). The sign of the effective mass of one of H_1 changes sign to positive value. As the lattice constant increases the

direct exchange responsible for the negative mass decays faster than the substrate mediated interaction, which wins the overall positive sign of the effective mass. The most dispersive side carbon bands H_4 and L_1 have smaller bandwidth by a factor of 2.5. The side carbons of 18% tilted SAM on Au are separeted by separated by 3.13 Åon neighboring molecules, whereas to the top and next to sulfur carbons are 5.0 Åapart. The occupied surface state SS_{occ} is strongly hybridized with the Sulfur p orbitals.

The molecular orbitals closest to the Fermi level are essential for the conductance properties of the monolayer. As in the case of Cu substrate the closest molecular orbital is HOMO due to the sulfur p orbitals. In order to enhance the hole current it is desirable to reduce the charge injection energy the energy difference between the Fermi level in the substrate and the energy of the first HOMO. We find lateral dispersion significant enough to modify conductance properties of the monolayer compared to the single molecule conductor. In order for the hole conductance of SAM to be more efficient then a single molecule the injection energy has to be effectively smaller or in other words the effective mass has to be positive. There are two contributions to the lateral dispersion with different next neighbor distance dependences: (1) a direct wavefunction overlap (2) substrate mediated superexchange type interaction. We can separate the relative contributions to the effective mass of $H_{1,2}$ by comparing the lateral dispersions obtained for the arrays of the thiophenolates in the absence of the substrates shown on Fig. (4) for the same geometries as on Cu(111) and Au(111) substrates.

The results of two calculations shown on Fig. 4 are similar. The dispersion of the molecular states is smaller for the Au(111) case Fig. (4, b) and so it is easy to analyze. The analysis of the bands with the substrate removed is given in table I and uses the same labeling for direct comparison. The sulfur $H_{1,2}$ bands have both negative effective masses with the bandwidths larger for the Cu geometry. In both cases the dispersion of the sulfur bands is larger in the absence of the substrate. This suggests that substrate mediated interactions has the opposite effect on the bandwidth then a direct exchange. When the lattice constant gets larger for Au, the substrate mediated interaction changes the one of the sulfur bands H_1. The coupling of the side phenyl carbons to the substrate is much smaller then the sulfur orbitals, which suggests that substrate mediated interaction of those bands (H_4 L_1,) is much weaker. The bandwidths change by less than 10%.

band	E_Γ (eV)		m_{eff} (m_e)		E_M-E_Γ (eV)		Character
	SAM/Cu	SAM	SAM/Cu	SAM	SAM/Cu	SAM	
H_4	-4.0	-3.6			3.7	3.86	C_{side}
H_3	-2.7	-1.9		-1.5			C_{top}
H_2	-1.1	0.30	-2.0	-1.0			S
H_1	-0.75	0.35	-2.0	-1.2		-0.88	S
L_1	1.0	1.6	0.4	0.35	3.8	3.8	C_{side}
L_2	2.8	3.7	-0.4	1.0			C_S
L_3	4.0	5.0	-0.3	-0.8	-1.8	-2.0	C_{top}
SS_{occ}	-0.9		0.4				Cu
SS_1	1.7						Cu
	SAM/Au	SAM	SAM/Au	SAM	SAM/Au	SAM	
H_4	-2.4	-2.2	0.55	0.8	1.6	1.5	C_{side}
H_3	-2.4	-2.1				-0.2	$C_{S,top}$
H_2	-0.98	0.13	-2.3	-2.7		-0.2	S
H_1	-0.85	0.09	1.6	-3.9		-0.3	S
L_1	2.75	2.9	1.0	0.95	1.2	1.1	C_{side}
L_2	4.1	3.9		0.9			$C_{S,top}$
L_3	4.1	4.3	-0.6	-1.2		-1.0	$C_{S,top}$
SS_{occ}	-0.45		1.7				Cu
SS_1	1.4		0.5				Cu

TABLE I: Analysis of the electronic bandstructure for SAM on Cu(111) SAM on Au(111) and free molecular arrays at the same geometries. The energies of the bands are given relative to the Fermi level at the Γ-point ($k = (0, 0, 0)$). Effective masses are reported for the bands where parabola fit (along the Γ-M direction) is possible. The bandwidth is reported for bands where the energy difference between the M and the Γ point can be identified. The last column shows the band character.

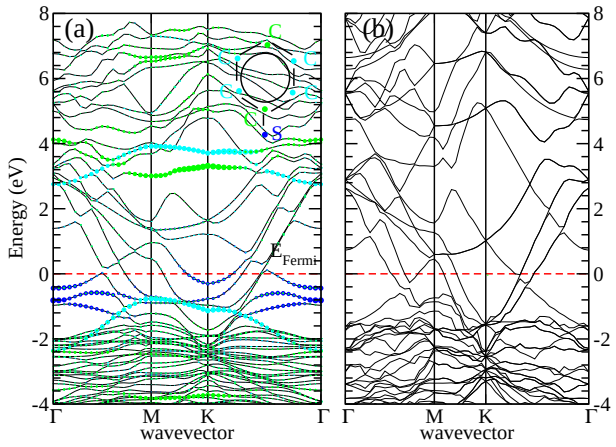

FIG. 3: (a) Band structure results for the SC_6H_5 SAM on 3 layers of Au(111). The size of the colored circles is proportional to the projected density of states of each bend on a given atom of a molecule (sulfur S-blue, next and top carbon $C_{1,4}$-green, phenyl ring carbons $C_{2,3,5,6}$-light blue). (b)Band structure of the 3 layer slab of Au(111). From comparison two HOMO and two LUMO's can be identified due to the SAM attachment.

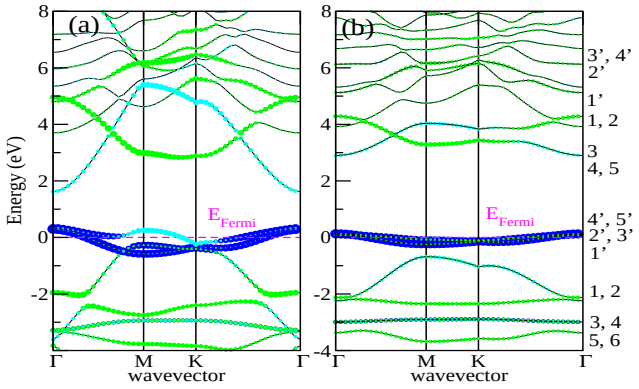

FIG. 4: (a) Band structure of the free standing array of SC_6H_5 at Cu(111) lattice constant and (b) a tilted by 18^0 thiophenolate array at Au(111) lattice constant.

IV. 2PPE SPECTRA

The electronic structure of the organic SAM can be directly probed in the photon photoemission experiment [10]. If the photon energy is less then the work function, then at least two photons has to be absorbed to removal an electron. By changing the energy of the incoming photon and looking at the position of the resonance one can identify whether the resonant electronic level due to the SAM is occupied, empty below the vacuum level or

empty above the vacuum level. In particular, for the thiophenolate S-C_6H_6 on Cu(111) two resonance A and B were resolved [1]. The energy position of A resonance is independent of the photon energy and therefore it is due to the final state above the vacuum level (6.4 eV above E_{Fermi}). Whereas peak position of the B resonance is linear with photon energy and therefore it is due to the resonant empty level below the vacuum (3.3 eV above E_{Fermi}). In the present studies we can identify second LUMO L_2 at 2.8 eV of the carbon next to sulfur character Fig. 2 and Table I. This character assignment is consistent with the conclusion drawn in [1] based on experimental peak positions of resonance B and cluster calculations of the different lengths alkanethiolates on Cu(111). There is no well defined molecular level in Fig. 2 at the expected position of the resonance A (at 6.4 eV). However, from the band count in Fig. (2, a) and Fig. (2, b) we can few extra bands around 6.0 eV on Fig. (2, a), which are due to the SAM. In order to identify which states contribute to the observed resonance A in [1] we should use dipole matrix element information in addition to the energies of the molecular levels. In particular, in the one photon process light couples *via* the dipole matrix elements which we compute between the each pair of DFT occupied $|i>$ and empty $|j>$ orbitals at $k = (0, 0, 0)$:

$$M_\alpha \ = \ \sum_{i<j} |< i|p_\alpha|j >|^2 \, f_i(1 - f_j)\delta(\hbar\omega - E_j + E_i), \qquad (1)$$

where $f_{i,j}$ occupation numbers for levels i and j. The results for the polarization parallel to the surface normal M_z and the in-plane polarization $(M_x + M_y)/2$ with Gaussian broadened delta functions are shown on Fig. (5). The dipole matrix elements between most of the orbitals are zero or negligible by symmetry or spacial delocalization of the wavefunctions. There are three distinct peaks in dipole matrix elements for z polarization: the first one at 2.6 eV is due to the transition between the occupied and the empty surface states; the second one is due to the transition between the occupied surface state and the second LUMO L_2 and the third one due to the transition from the first HOMO H_1 and some high energy Cu state at about 3.8 eV. Those peak would result in intensity resonances of the observed spectra. In particular, at the laser frequency ω_L 3.7 eV the L_2 level will be resonant, whereas surface state will be resonantly populated at ω_L 2.6 eV and for ω_L 4.6 eV the first HOMO H_1 will be resonant. For the in-plane polarization the dipole matrix elements are smaller and the low energy resonances are associated with transition between the H_1 and L_1 levels at 1.7 eV; H_1, H_2 and SS_1 at 2.4 and 2.8 eV correspondingly; and between the H_3 and L_1

levels at 3.6 eV. One has to keep in mind that in order to see the electron emitted from the populated level the energy of the second photon has to be enough to remove an electron from the populated level to the vacuum. There are two mechanisms which give rise to the 2PPE intensity (see for example [10]). In the direct mechanism the first photon excites an electron from the occupied metal state to the empty molecular state. The second photon ionizes the molecular anion. The intensity of the 2PPE [11, 12] for the one-color experiment is:

$$\mathrm{I}_{\alpha}^{\mathrm{dir}}(i,f,\omega_L) \;\sim\; \delta(2\hbar\omega_L - \mathrm{E}_f + \mathrm{E}_i)\left|\sum_{i<m<f}\frac{<f|p_\alpha|m><m|p_\alpha|i>}{\mathrm{E}_m - \mathrm{E}_i - \hbar\omega_L + i\Gamma_m}\right|^2 f_i(1-f_m) \qquad (2)$$

where Γ_m is the lifetime broadening of intermediate level m. The sum over intermediate states in Eq. 2 includes the interference effects. The delta function is replaced by the Lorentzian to mimic the lifetime of the final state and the laser frequency uncertainty of the pulsed lasers.

In the second indirect mechanism the intermediate level is populated by some incoherent process for example by the tunneling of the photoexcited electron in the substrate to the molecule. The second photon removes an photoexcited electron to the vacuum with the probability given as in the one photon absorption process:

$$\mathrm{I}_{\alpha}^{\mathrm{indir}}(m,f,\omega_L) \;\sim\; \delta(\hbar\omega_L - \mathrm{E}_f + \mathrm{E}_m)\,|<f|p_\alpha|m>|^2\,(1-f_m)(1-f_f)f_m(\mathrm{E}_{\mathrm{Fermi}} + \hbar\omega_{\mathrm{L}}) \quad (3)$$

where $(1-f_m)$ and $f_m(E_{Fermi}+\omega_L)$ factors requires that the intermediate state is empty in equilibrium and has equal probability to be excited with a single photon, if its energy is less then $\hbar\omega$ away from Fermi level. The different lifetimes of the intermediate and final states in the direct mechanism and the deviation from the uniform population of intermediate states below $\hbar\omega$ may lead to the corrections of the present results.

In the present work we are going to study the effect of the dipole matrix elements on the two photon photoemission spectra. On Fig. 6 we plot the sum of the probabilities given by (Eq. 2) to excite the final state f over all the initial states i *versus* the final state energy E_f for the plane normal and the in-plane polarizations. The calculated curve were convoluted with a Lorentzian function ($\Gamma = 0.1$ eV) to account for the spectrometer resolution. We use $\Gamma_m = 0.1$ eV for the intermediate level damping and the replace delta-function in Eq. 2 by Lorentzian with the same value $\Gamma_f = 0.1$ eV to account for the lifetime of the final state. There is one pronounced peak at about 6.0 eV, which intensity

is resonant with the laser frequency at about 3.6 eV. As the frequency increases the states at high energies at about 7 eV gets excited with a diminishing probability to excite 6 eV HOMO's. The resonance enhancement factor is sensitive to the choice of the damping parameters and even for the large value of 0.1 eV used in Fig. 6 the intensity of the out-of-plane polarization varies by the order of magnitude. The resonance effect is related to the large dipole matrix element between the occupied surface state and the second LUMO L_2 separated by 3.7 eV. For the larger laser frequency higher energy states at 7 eV could be excited with the decaying probability to excite 6 eV LUMO. For the in-plane polarization there is no strong frequency dependence of 2PPe intensity, because there is no particular pair of states which dominate the sum in Eq. 2. Therefore the ratio of the out-of-plane and the in-plane polarizations should be very sensitive to the laser frequency, if the direct mechanism would be dominate. Similar calculations for the 2PPE intensity were done for the indirect mechanism (Eq. 3) assuming the same population rate of all the intermediate states. The results for two polarizations and the same damping parameters are shown in Fig. 7. There are no pronounced resonances observed for the indirect mechanism. The ratio of the out-of-plane and the in-plane polarizations is relatively independent on laser frequency. The ratio of the integrated peak intensities at 6 eV for ω_L =3.4, 3.5, 3.7, and 3.9 are 1.8, 4.6, 3.8, and 4.0 respectively. This is in agreement with the experimentally report value of $I_p/I_s \approx 4$ at $\omega_L = 3.7$ eV [1]. The analysis based on the dipole matrix element effect makes us to conclude that most likely mechanism for the two photon photoemission intensity is an indirect, where the intermediate molecular state is populated as a result of the single photon absorption and the consequent electron emission due the second photon absorption.

V. WORK FUNCTION CALCULATION

The change of the work function due to the SAM may be employed in electronic device application to align the Fermi level of the metal to the valance or conduction bands in carbon nanotubes [13]. It is very important to have a realistic tool to make a quantitative prediction of the change in the workfunction due the SAM adsorbate. The work function of a crystal is the minimum energy required to remove an electron from deep within the bulk to a point a macroscopic distance outside the surface. More precisely,

$$\Phi = \upsilon(\infty) - E_{\text{Fermi}}, \tag{4}$$

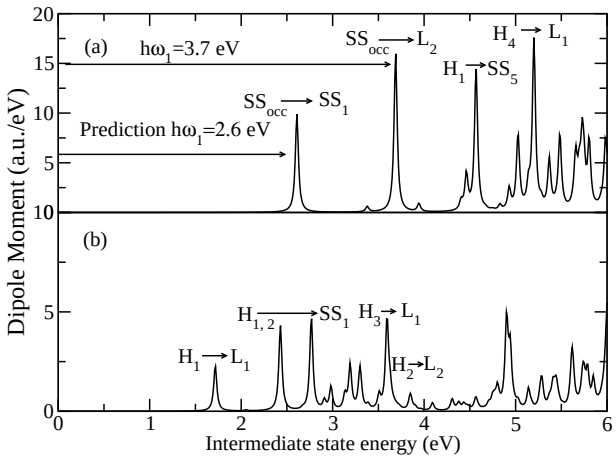

FIG. 5: Calculated dipole matrix elements between all possible pairs of occupied and unoccupied states for the two light polarizations parallel (a) to the surface normal (b) and for the in-plane polarization versus energy differences.

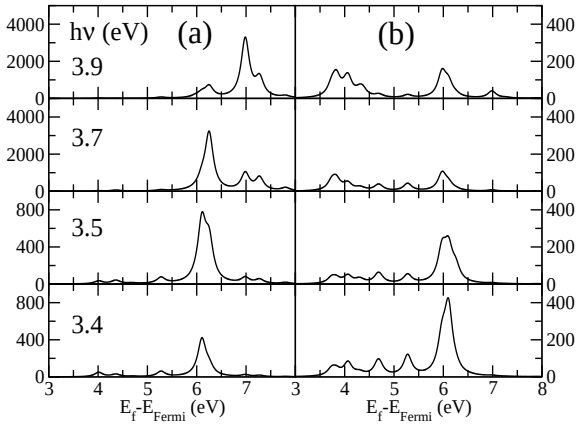

FIG. 6: Prediction of the two photon photoemission spectra according to Eq. (?) for $k = (0, 0, 0)$.

where $\upsilon(\infty)$ is the electrostatic potential far from the surface and E_{Fermi} is the bulk chemical potential. There are two contributions to the work function [14] the electrostatic barrier due to the surface dipole and the many-body effects of the screened hole. The electrostatic contribution follows from the Poisson equation:

$$\upsilon(\infty) - \upsilon(0) = 4\pi \int_0^\infty z[\rho(z) - \rho_+(z)]dz, \tag{5}$$

provided the charge neutrality of the slab is satisfied $\int_0^\infty [\rho(z) - \rho_+(z)]dz = 0$, where ρ and ρ_+ are the electron and nuclear charge densities. The many-body effects are contained in the exchange and correlation contributions to E_{Fermi}.

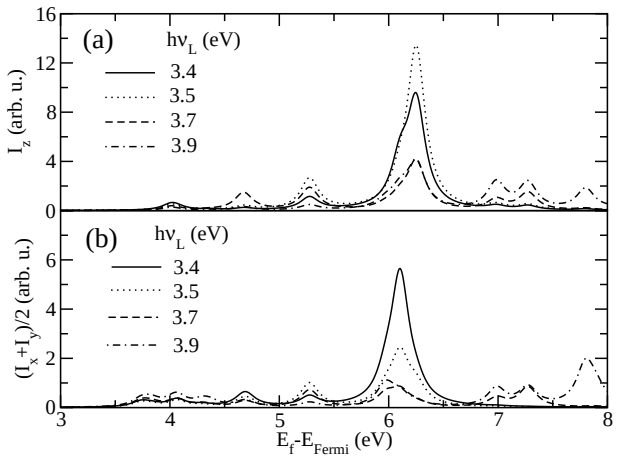

FIG. 7: Substrate assistant 2 photon photoemission spectra calculations.

The slab of three metal layer with one side covered by SAM has a permanent non-zero dipole which induces a constant electric field in the vacuum region, such that the Coulomb potential $v(\infty)$ can be found uniquely. For the work function calculations we increased the metallic Cu substrate to six layeres and covered it from the both sides. The inversion symmetry of the slab forces the net dipole to be zero. The Coulomb potential of the two sided covered six layer Cu(11) substrate is shown on Fig. 8 along with clean substrate and two SAM arrays in the absence of the substrate. The work function of the clean Cu(111) is found to be 5.0 eV in a good agreement with experimental value of 4.9 eV. The work function of the covered substrate is reduced to 2.7 eV, whereas experimental value is 3.7 eV [1]. To separate the electrostatic and exchange correlation contributions to the work function we calculate the surface dipole by integrating the charge density of the half the unit cell:

$$P = \int_0^{z/2} z[\rho(x,y,z) - \rho_+(x,y,z)]dxdydz. \tag{6}$$

The ratio of Coulomb potential difference across the single layer of SAM in a free space (Fig. 8, b) over the $4\pi P_{SAM}$ is 1.01. The ratio of the work function to the electrostatic contribution are 1.09 and 1.51 for clean Cu(111) and SAM/Cu(111) respectively. The dipole per S-C_6H_6 molecule in the SAM array is P_{SAM}=1.19 Debye, whereas a dipole of the single molecule of the same geometry calculated with NRL code [15] gave a significantly larger value 3.33 Debye. The band formation in the molecular array lead to the redistribution of the valance charge density on the molecule which caused a much smaller effective dipole moment. In addition the long range Coulomb interaction creates an effective electric field which reduces

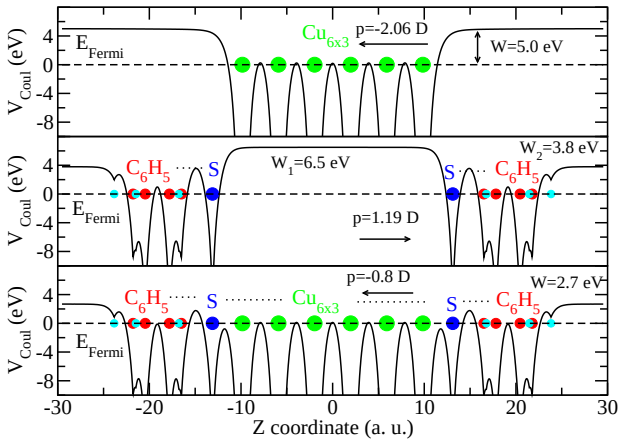

FIG. 8: Work function and surface dipole calculations for the clean Cu(111) (a), single monolayer (b) and SAM on Cu(111) (c).

the dipole moment of the molecule by the amount proportional to its polarizability. For the intermediate coupling controlled by the distance between the molecules it is hard to separate the relative strength of the two effects, which are taken into account in DFT supercell approach on the same footing.

When the covalent bond is formed between the sulfur and the noble metal the charge transfer takes place. On fig. 9 we show the charges densities integrated over the xy plane versus the plane normal direction for the three runs of calculations of clean Cu(111), two SAM arrays with no substrate, and the double sided SAM/Cu(111). The charge density change due the adsorbate shown on Fig. (9, b) is very small, such that charge transfer between the molecule and the substrate of less then 0.1 e takes place. The corresponding dipole moment due the charge transfer is only 0.076 Debye per molecule. This implies that electrostatic contribution to the work function change can be estimated with degree of accuracy by calculating the dipole moment of the free standing array of molecules.

VI. SUMMARY

We have calculated electronic structure of the SAM thiophenolate (S-C_6H_5) on Cu(111) and Au(111) substrates. We found the sulfur HOMO (H_1) to the closest to the Fermi level in both cases and therefore the hole channel is expected to contribute the most to the current in the presence of the bias. We identified four HOMO's and three LUMO's for the both

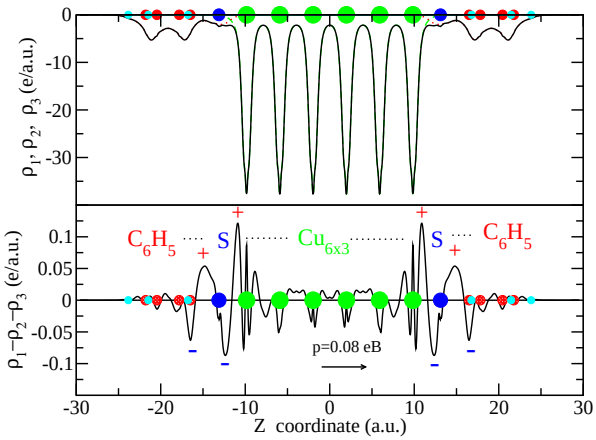

FIG. 9: (a) Charge density versus z-direction of the Cu(111) (blue), free SAM (red) and attached SAM/Cu(111) (black). (b) Results for the charge density difference and the induced dipole at the contact due to the charge transfer p=0.08 (D).

systems. The most dispersive molecular bands are of the side carbon atoms character. For the most important sulfur bands we found two competing contributions to the dispersion: (1) the direct wavefunction overlap to give a negative effective mass (2) the substrate mediated interaction to give a positive effective mass. The overall sign of the effective mass is changed by going from Cu to Au substrate due to the different molecule separation dependence of the two interactions.

The dipole matrix element informations allowed us to identify which of the molecular states were observed in the experiment of Zhu group [1] on thiophenolate on Cu(111). The resonance A seen at 6.4 eV in [1] is calculated at 6.0 eV and the resonance B observed at 3.4 eV is found due to the LUMO L_2 at 2.8 eV. Those molecular states are mainly due to the character next to sulfur and top carbon atoms. We made the calculations of the resonance A for the direct and indirect mechanisms. For the out-of-plane polarization in the direct mechanism we found the transition between the occupied surface states and the L_2 state contributes the most intensity into 2PPE intensity. In particular, the order of magnitude intensity enhancement is predicted for the resonance A is the direct mechanism is dominant. For the in-plane light polarization contributions due the transitions between several pairs of states in the first step are comparable and only moderate resonance A intensity variation with laser frequency is found. In the indirect mechanism all the intermediate states below the laser frequency are supposed to be equally occupied. The result of calculations suggests

moderate variation of the resonance A intensity with a nearly constant ratio of the out-of-plane to in-plane signals around the experimental value 4. This makes us to conclude that the indirect mechanism contributes the most intensity in to the 2PPE peak intensity of resonance A observed in [1].

The calculations of the work function due to the SAM coverage of Cu(111) predicts underestimated value of 2.7 eV compared to the experimental value of 3.7 eV. We find electrostatic contribution to the work function change 1.8 eV and it is nearly effected by the charge transfer between the molecules and the substrate, which is very small and introduces only a 10% correction to the electrostatic contribution. On the other hand we find almost 3 times larger dipole moment of the free standing molecule compared to the dipole per molecule in the array pinned to the Cu lattice constant.

Our results suggest the charge injection energy is largely modified due to the lateral dispersion of the corresponding molecular band. The conductance properties depends exponentially on the charge injection energy and therefore conductance of the monolayer can not be determined from the single molecule conductance. In addition we identify the the relative contribution of the two mechanisms which lead to the lateral dispersion of the sulfur HOMO. This may be used to fictionalize the conductance properties of the monolayers by changing the underlying substrates or the coverage of the SAM.

Acknowledgments

The computations were performed on the BNL galaxy cluster. We are grateful to Mike Weinert for helpful discussions. This work was supported in part by DOE Grant No. DE-AC-02-98CH10886.

---

[1] T. Vondrak, H. Wang, P. Winget, C. J. Cramer, and X.-Y. Zhu, J. Am. Chem. Soc. **122**, 4700 (2000).

[2] D. J. Singh, *Planewaves, Pseudopotentials and the LAPW Method* (Kluwer Academic, Boston, 1994).

[3] D. J. Singh, Phys. rev. B **43**, 6388 (1991).

[4] P. Blaha, K. Schwarz, and J. Luitz, in *Proceedings of WIEN97* (Techn. Universität Wien, Austria, 1999).

[5] J. P. Perdew and Y. Wang, Phys. Rev. B **45**, 13244 (1992).

[6] *See review by* F. Schreiber, Prog. in Surf. Sci. **65**, 151 (2000).

[7] T. Y. B. Leung, P. V. Schwartz, G. Scoles, F. Schreiber, A. Ulman, Surf. Sci. **458**, 34 (2000).

[8] M. C. Vargas, P. Giannozzi, A. Selloni, and G. Scoles, J. Phys. Chem. B **105**, 9509 (2001).

[9] A. Euceda, D. M. Bylander, and L. Kleinman, Phys. Rev. B **28**, 528 (1983)

[10] X.Y. Zhu, Annu. Rev. Phys. Chem. **53**, 221 (2002).

[11] O. Madelung, in *Introduction to Solid-State Theory*, edited by M. Cardona, P. Fulde, and H.-J. Oueisser (Springer Series in Solid-State Sciences **2**, Springer, Berlin 1981) p. 276.

[12] M. Wolf, A. Hotzel, E. Knoesel, and D. Velic, Phys. Rev. B **59**, 5926 (1999).

[13] X. Cui, M. Freitag, R. Martel, L. Brus, and P. Avouris

[14] N. D. Lang, in *Solid State Physics*, edited by Seitz, Turnbull, and Ehrenreich **28** Academic Press, New York 1973 p. 225.

[15] M. R. Pederson and K. A. Jackson, Phys. Rev. B. **41**, 7453 (1990); K. A. Jackson and M. R. Pederson, Phys. Rev. B. **42**, 3276 (1990); M. R. Pederson and K. A. Jackson, Phys. Rev. B. **43**, 7312 (1991); D. V. Porezag and M. R. Pederson, Phys. Rev. B. **54**, 7830 (1996); A. Briley, M. R. Pederson, K. A. Jackson, D. C. Patton, and D. V. Porezag, Phys. Rev. B. **58**, 1786 (1998).